doi:10.1016/j.jmb.2012.01.034 J. Mol. Biol. (2012) 421, 587–600

Contents lists available at www.sciencedirect.com

Journal of Molecular Biology

journal homepage: http://ees.elsevier.com.jmb

Disease-Associated Polyglutamine Stretches in Monomeric Huntingtin Adopt a Compact Structure

Clare Peters-Libeu[1,2], Jason Miller[1,3,4]†, Earl Rutenber[1,2]†, Yvonne Newhouse[1,2], Preethi Krishnan[1,5], Kenneth Cheung[1,5], Danny Hatters[1,2], Elizabeth Brooks[1,5], Kartika Widjaja[1,5], Tina Tran[1,5], Siddhartha Mitra[1,3,6], Montserrat Arrasate[1,3], Luis A. Mosquera[7], Dean Taylor[8], Karl H. Weisgraber[1,2,8] and Steven Finkbeiner[1,3,5,9,10]*

[1]*Gladstone Institute of Neurological Disease, San Francisco, CA 94158, USA*
[2]*Gladstone Institute of Cardiovascular Disease, San Francisco, CA 94158, USA*
[3]*Medical Scientist Training Program, University of California, San Francisco, CA 94141, USA*
[4]*Chemistry and Chemical Biology Program, University of California, San Francisco, CA 94141, USA*
[5]*Neuroscience Program, University of California, San Francisco, CA 94141, USA*
[6]*Biomedical Sciences Program, University of California, San Francisco, CA 94141, USA*
[7]*Sunol Molecular Corp., Miramar, FL 33025, USA*
[8]*Department of Pathology, University of California, San Francisco, CA 94143-0506, USA*
[9]*Department of Neurology, University of California, San Francisco, CA 94143, USA*
[10]*Department of Physiology, University of California, San Francisco, CA 94143, USA*

Received 22 September 2011; received in revised form 18 January 2012; accepted 21 January 2012
Available online 28 January 2012

Edited by S. Radford

Keywords:
Huntington's disease; huntingtin structure; polyglutamine expansion; amyloid; antibody

Abnormal polyglutamine (polyQ) tracts are the only common feature in nine proteins that each cause a dominant neurodegenerative disorder. In Huntington's disease, tracts longer than 36 glutamines in the protein huntingtin (htt) cause degeneration. *In situ*, monoclonal antibody 3B5H10 binds to different htt fragments in neurons in proportion to their toxicity. Here, we determined the structure of 3B5H10 Fab to 1.9 Å resolution by X-ray crystallography. Modeling demonstrates that the paratope forms a groove suitable for binding two β-rich polyQ strands. Using small-angle X-ray scattering, we confirmed that the polyQ epitope recognized by 3B5H10 is a compact two-stranded hairpin within monomeric htt and is abundant in htt fragments unbound to antibody. Thus, disease-associated polyQ stretches preferentially adopt compact conformations. Since 3B5H10 binding predicts degeneration, this compact polyQ structure may be neurotoxic.

*Corresponding author. Gladstone Institute of Neurological Disease, San Francisco, CA 4158, USA. E-mail address: sfinkbeiner@gladstone.ucsf.edu.

† These authors made equal contributions.

Present addresses: C. Peters-Libeu, Buck Institute, Novato, CA 94925, USA; P. Krishnan, College of Pharmacy, University of Minnesota, Minneapolis, MN 55455, USA; K. Cheung, University of California School of Medicine, Sacramento, CA 95817, USA; D. Hatters, Department of Biochemistry and Molecular Biology, The University of Melbourne, Melbourne, VIC 3010, Australia; E. Brooks, Neuroscience Program, University of California School of Medicine, Los Angeles, CA 90095-1761, USA; M. Arrasate, Division of Neuroscience, CIMA, University of Navarra, Avda. PíoXII, 55, E-31008 Pamplona, Spain; L. A. Mosquera, VaxDesign Corp., Orlando, FL 32826, USA; D. Taylor, Altor Bioscience Corp., Miramar, FL 33025, USA.

Abbreviations used: polyQ, polyglutamine; htt, huntingtin; wt, wild type; HA, hemagglutinin; IP, immunoprecipitation; PDB, Protein Data Bank; CDR, complementarity-determining region; SAXS, small-angle X-ray scattering; Cer, Cerulean fluorescent protein; MBP, maltose binding protein.

0022-2836/$ - see front matter

Introduction

An abnormal expansion of the polyglutamine (polyQ) tract in huntingtin (htt) results in a self-aggregating protein and neurodegeneration. Understanding which structures of polyQ in mutant htt and other polyQ-expanded proteins are most closely linked to pathogenesis has important implications for mechanisms of neurotoxicity. For example, unaggregated expanded polyQ has been suggested to mediate toxicity through aberrant recruitment of cellular proteins.[1] If such "recruitment-competent" polyQ is structured, then mutant htt may act as a structural mimic/competitor for the recruited protein's normal binding partners. Alternatively, if "recruitment-competent" polyQ is unstructured, then expanded polyQ may simply provide a longer, more accessible recruitment site than wild-type (wt) stretches of polyQ.

These alternate pathogenic scenarios lead to potentially divergent therapeutic strategies. In the case of a structured polyQ epitope, screens for therapeutics that disrupt toxic structure formation may be warranted. In the case of an unstructured polyQ epitope, therapeutic strategies may instead focus on covalently linking together multiple copies of a molecule that recognizes a short linear array of polyQ.[2–5]

While the structure of aggregated polyQ peptides takes on the classical cross-β-strand structure of amyloid fibrils,[6] the exact structures and pathogenic significance of a range of putative monomeric species and very small oligomeric species of mutant htt are unknown. The first exon of wt htt was recently crystallized, revealing multiple conformations of the polyQ stretch.[7] However, studies on expanded (mutant) polyQ suggest that the unaggregated forms are largely unordered, adopting secondary structure only upon aggregation.[5,8,9] These data led to the concept of "beads on a string," a linear sequence of unaggregated glutamines without secondary structure. In this "linear lattice" model, the toxicity of unaggregated expanded polyQ is caused by an increased accessibility of the polyQ region to cellular ligands.[2,5] Furthermore, if a particular cellular ligand has two polyQ binding sites, then the ligand will exhibit a strong preference for expanded over wt stretches of polyQ driven by increased avidity. Indeed, at least two IgG antibodies (MW1 and 1C2), which inherently have two identical epitope binding sites, have been thought to preferentially bind expanded polyQ, at least in part, by the avidity mechanism implied in the "linear lattice" model.[2,10]

In contrast to the "linear lattice" model, some pieces of *in vitro* experimental evidence indicate that expanded polyQ induces a global change in conformation in unaggregated htt.[1,11,12] However, direct experimental evidence indicating that disease-associated polyQ stretches adopt an emergent conformation *in situ* is lacking. Furthermore, whether any particular emergent conformation formed *in situ* is toxic is also unknown.

We identified a monoclonal antibody, 3B5H10, that recognizes a species of htt in neurons that predicts neurodegeneration better than all other α-htt antibodies tested, including the "linear-lattice"-recognizing antibody MW1.[13] Here, we show that 3B5H10 recognizes a compact two-stranded conformation of polyQ in monomeric htt that emerges when the polyQ stretch expands. Our data show that a specific compact conformation of expanded polyQ forms in unaggregated htt *in situ* and that this compact conformation has particular pathological significance.

Results

Monoclonal 3B5H10 recognizes a structured polyQ epitope in a fragment of htt

Since the epitope recognized by monoclonal antibody 3B5H10 predicted neurodegeneration better than the epitope recognized by MW1,[13] we considered the possibility that 3B5H10 recognizes an epitope formed preferentially by mutant htt rather than a repeated epitope envisioned by the linear lattice model. We reasoned that a conformation that preferentially forms in mutant htt should be stable at disease-associated polyQ lengths, unstable at near-threshold lengths, and relatively unformed at short lengths.

To test this putative difference in stability, we probed the effects of the denaturant SDS on 3B5H10 binding to mutant, threshold, and wt versions of htt. Specifically, we chose to test three different polyQ stretches (Q_{17}, Q_{25}, and Q_{40}) based on the frequency with which the corresponding CAG codon stretches are found in the htt gene within humans. A stretch of Q_{17} is among the most common alleles found in the normal population,[14–17] whereas a stretch of Q_{40} is relatively common among Huntington's disease patients and is fully penetrant.[15,17] Htt alleles with $Q_{23–34}$ are relatively rare but correspond to a transition zone between the most common normal alleles and disease-associated alleles and, therefore, may have particularly interesting biochemical properties.[15,17]

Cells were transfected with N-terminal 171-amino-acid fragments of htt containing 17, 25, or 40 polyQ stretches, as well as hemagglutinin (HA) and FLAG epitope tags fused, respectively, to the N-terminus and C-terminus of htt. Cells were lysed under native conditions 48 h after transfection, and lysates were immunoprecipitated with α-HA

epitope or 3B5H10 antibodies, subjected to SDS-PAGE, and blotted with α-HA epitope or 3B5H10 antibodies. When the lysates were subjected to immunoprecipitation (IP) and blotting with α-HA antibody, the three versions of htt showed equal immunoblotting intensities, signifying that all were equally available for IP (Fig. 1a). In contrast, IP with 3B5H10 and blotting with α-HA antibody revealed a band for the Q_{40} and Q_{25} versions of HA-171-Htt-FLAG, but not for the Q_{17} version. This finding confirms that 3B5H10 preferentially binds to versions of htt near the threshold or higher. Interestingly, when the three versions of htt were immunoprecipitated with 3B5H10 and then blotted with 3B5H10, only HA-171-Q_{40}-FLAG was detected. This suggests that the epitope on HA-171-Q_{25}-FLAG recognized by 3B5H10 was unstable and disappeared upon SDS exposure, while the HA-171-Q_{40}-FLAG epitope recognized by 3B5H10 remained. Since some proteins demonstrably retain or regain substantial secondary structure on a nitrocellulose membrane after SDS-PAGE,[18–26] immunoreactivity to HA-171-Q_{40}-FLAG after SDS exposure does not exclude the possibility that 3B5H10 recognizes a protein fold. These results deviate from simple predictions of the "linear lattice" model and suggest that 3B5H10 recognizes an epitope that is sensitive to SDS denaturation and whose sensitivity varies in a polyQ-length-dependent manner.

Crystal structure of 3B5H10

Since our data suggested that 3B5H10 recognizes a conformation of polyQ that emerges with longer polyQ stretches, we sought to characterize the structure of this conformation. First, we visualized 3B5H10's epitope binding groove by purifying[26] and crystallizing[27] its Fab fragment. We determined its X-ray crystal structure at 1.9 Å resolution by single isomorphous replacement with anomalous scattering and molecular replacement [Protein Data Bank (PDB) ID: 3S96] (Fig. S1, Tables S1–S3). During the process of solving the structure, we noticed several similarities between 3B5H10 and MW1. For example, both antibodies have a λ light chain, which is found in only 5% of the mouse antibody repertoire.[28] Furthermore, a sequence comparison of 3B5H10 and MW1 reveals nearly identical light-chain complementarity-determining regions (CDRs) and highly similar heavy-chain CDRs that are particularly enriched in aromatic residues (Fig. 1b), many of which are solvent accessible (yellow; Fig. 1c and d). Consistent with aromatic moieties facilitating glutamine binding,[3,29,30] 33% and 30% of the residues in the heavy-chain CDRs of MW1 and 3B5H10, respectively, are aromatic, in contrast to 9% of residues for the heavy-chain CDRs of the 100 closest homologues.

A surface representation of 3B5H10 Fv reveals a potential polyQ epitope binding groove studded with regularly spaced aromatic residues that stretches diagonally across the antibody's CDRs (Fig. 1c). The diagonal orientation of the potential epitope binding groove, which is also seen in the crystal structure of MW1 Fv (Fig. 1d), is unique among 48 other antibody/peptide structures surveyed from the PDB.[2] Previous studies of a $GQ_{10}G$ peptide complexed with MW1 Fv (PDB ID: 2OTU)[2] revealed that the polyQ peptide follows the path of solvent-accessible aromatic residues in the diagonal epitope binding groove (Fig. 1e). Upon peptide binding, the groove straightens through a 3° rotation between the antibody's heavy and light variable chains (domain rotation) to accommodate the uncurved epitope.

The strong sequence and structural similarities between MW1 and 3B5H10 suggested that polyQ binds to 3B5H10 along the analogous diagonal groove, taking advantage of regularly spaced aromatic residues lining the groove. Furthermore, the strong similarities suggest that the 3° domain rotation seen in MW1 upon epitope binding also occurs in 3B5H10. Such domain rotations are observed for other antibody/epitope interactions and are well-documented in the literature.[31] Indeed, alternative crystal forms of 3B5H10 Fab (PDB ID: 4DCQ) were consistent with this domain rotation (Fig. S2e and Supplementary Discussion). Analogous to MW1, this domain rotation straightens the epitope binding groove of 3B5H10 Fv while producing minimal steric clash. Among all residues at the heavy-chain/light-chain interface after domain rotation, only seven are needed to adopt an alternate side-chain rotamer involving at least a 1-Å shift for at least one atom in the residue. No atom shifted by greater than 1.6 Å (Fig. S2, Supplementary Discussion, and Supplementary Methods).

The epitope binding grooves of 3B5H10 and MW1 have different widths

While MW1 Fv and 3B5H10 Fv appear sequentially and structurally similar (Fig. 1), several key differences are observed when the crystal forms are overlaid on each other (Fig. 2a). 3B5H10 Fab has unusually long β-strands in CDR3 of the light chain (L-CDR3) and in CDR2 of the heavy chain (H-CDR2), unlike the corresponding CDRs of the Fv fragment of MW1 (Fig. 2a). Since MW1 and 3B5H10 share nearly identical light chains (Fig. 1b), differences in paratope conformation, particularly the packing interactions between H-CDR2 and L-CDR3 and between H-CDR2 and H-CDR1, are determined by the heavy chain (Fig. 2b–d). While the structure of L-CDR3 is loop like in MW1, it forms an extended β-hairpin that is observed in all crystal forms of 3B5H10 Fab, regardless of the location of crystal cell contacts. Although stable rigid secondary structures in CDRs are unusual, similar β-strands have been found in the CDRs of other Fabs.[32]

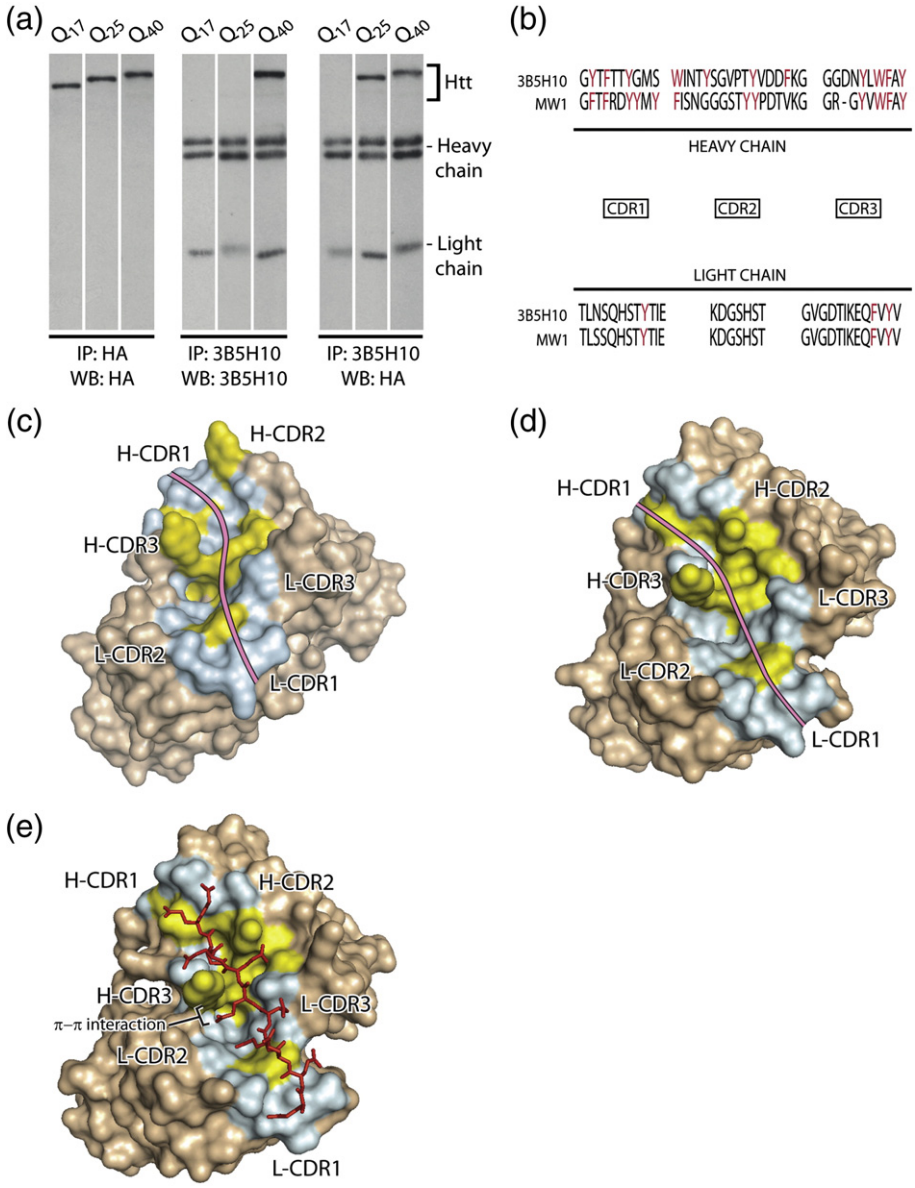

Fig. 1. Paratope structure for the conformation-specific polyQ antibody 3B5H10. (a) 3B5H10 is a conformation-specific antibody, recognizing a structure that is preferentially formed by disease-associated polyQ expansions. FLAG and HA-tagged N-terminal fragments of htt with polyQ stretches in the wt (Q_{17}), near-disease-threshold (Q_{25}), and disease-associated (Q_{40}) ranges were immunoprecipitated from cell lysates under native conditions. When immunoprecipitated with a-HA antibody, all three htt constructs were pulled down equally well, as shown by Western blot analysis with α-HA. However, when immunoprecipitated with the conformation-sensitive antibody 3B5H10, only htt with near-disease-threshold and disease-associated polyQ lengths were pulled down. When the same Western blot analysis was probed with 3B5H10 instead of α-HA, htt with a near-disease-threshold polyQ length was no longer detected, suggesting that this polyQ length has a relatively unstable conformation that denatures under the conditions used for Western blot analyses. These results are most consistent with 3B5H10 recognizing a conformation of polyQ that emerges as the polyQ tract expands. (b) CDR sequences of 3B5H10 and MW1. Aromatic residues are shown in red. (c) Likely paratope groove of 3B5H10 Fv (pale-red line). Solvent-accessible aromatic residues in the relatively wide groove are shown in yellow. Other residues in the floor and walls of the groove are shown in light blue. In the middle of the groove is a pocket containing two solvent-accessible tryptophans (see Fig. 3a). (d) Narrow valley in the paratope of unbound MW1 Fv (PDB ID: 2GSG), shown as in (c). (e) $GQ_{10}G$ peptide bound to MW1 Fv (PDB ID: 2OTU).[2] The polyQ peptide (red) follows the path of solvent-accessible aromatic residues (yellow) in the paratope valley (light blue). Upon peptide binding, the paratope path straightens through a 3° rotation between the antibody's heavy variable chains and the antibody's light variable chains (domain rotation) to accommodate the uncurved epitope. Note a π–π stacking interaction between Y102 from H-CDR3 and a glutamine from the peptide (black line).

In MW1, hydrogen bonds between L-CDR3 and H-CDR2 appear to stabilize the extended loop-like structure of L-CDR3 and bring L-CDR3 and H-CDR2 closer together to form part of the wall of the epitope binding groove (Fig. 2b and c). Because of sequence differences in H-CDR2 between MW1 and 3B5H10, these hydrogen bonds do not exist in 3B5H10. The overall effect of these differences is to convert a steep wall midway through the epitope binding groove in MW1 into a shallow, less rigid wall for 3B5H10 (Fig. 2b and c). This serves to make the diameter wider midway through 3B5H10's epitope binding groove, as compared to MW1.

The extended β-hairpin in H-CDR2 of 3B5H10 also prevents significant packing between H-CDR2 and H-CDR1, thereby contributing to the widening of the epitope binding groove at one end of the 3B5H10 paratope (Fig. 2b and d). In contrast, the more loop-like structure of MW1 H-CDR2 packs tightly against H-CDR1, contributing to a wall that significantly narrows the corresponding portion of the paratope valley in MW1 (Fig. 2b and d) and allows for only a single polyQ strand to bind. Indeed, the narrowest diameter of the peptide binding groove in MW1 spans from G101 in H-CDR3 to Y33 in H-CDR1 and measures 5.5 Å. In contrast, the narrowest diameter of the peptide binding groove in 3B5H10 spans from Y103 in H-CDR3 to N52 in H-CDR2 and measures 12.15 Å. Thus, the extended β-hairpin structure of H-CDR2 and its interaction with H-CDR1 and LCDR-3 in 3B5H10 result in a significantly wider groove across the length of 3B5H10's paratope, as compared to MW1.

A compact two-stranded hairpin conformation allows polyQ to fit into the 3B5H10 paratope

The width of 3B5H10's epitope binding groove, as compared to MW1, suggests that it binds to a larger/wider epitope than the single polyQ strand that binds MW1's paratope (see Fig. S3). Since β-strands are believed to be the fundamental secondary structural unit of compact polyQ structures,[33] we used flexible docking in ClusPro[34] and ZDOCK[35] to explore the compatibility of single-stranded and double-stranded β-rich polyQ conformations with 3B5H10 and MW1 (Supplementary Methods). This procedure replicated the crystal structure of a $GQ_{10}G$ peptide bound to MW1[2] and demonstrated that MW1 recognizes various polyQ models containing β-strands (Figs. S3 and S4). For all multistranded polyQ models complementary to MW1, only a single strand was inserted into the antibody's peptide binding groove, following the path of the bound $GQ_{10}G$ peptide (see Fig. S5 for an example). Thus, MW1 may bind additional conformations of polyQ besides the random-coil conformation described[2,5] (Supplementary Discussion).

In contrast, only two-stranded β-hairpin models customized to fit 3B5H10's paratope docked with 3B5H10 (Supplementary Discussion and Supplementary Methods). Attempts to dock single-stranded and double-stranded models position a glutamine directly over two solvent-accessible tryptophans in the paratope groove (Fig. 3a), consistent with a 5-nm redshift in tryptophan fluorescence when 3B5H10 binds a thioredoxin hexahistidine fusion protein of exon 1 of htt with 39 glutamines (Thio-Htt^{ex1}-Q_{39}-His_6) (Fig. 3b). However, single-stranded models fail to completely fill the binding surface, resulting in significantly fewer hydrogen bonds per square angstrom than in the MW1/$GQ_{10}G$ crystal structure (Fig. S3), double-stranded models (Fig. S4), or complexes of homologous Fabs and their antigens (Fig. S3). For double-stranded docking, we utilized the paratope from the 3B5H10 crystal structure in Fig. 1c and the paratope from the domain-rotated version of 3B5H10 discussed above. Docking results revealed that a β-rich hairpin model is complementary to the paratope of 3B5H10 observed in the crystal structure (Fig. 3c), whereas the domain-rotated paratope accommodates a flatter β-rich hairpin model (Fig. 3d). Each model aligned both β-rich strands roughly parallel with the binding surface, burying 950–1100 $Å^2$ and forming 12–16 hydrogen bonds well within the range for complexes of homologous Fabs and their protein antigens (Fig. S4). Thus, the epitope of 3B5H10 is a conformation of polyQ similar to a two-stranded β-rich hairpin.

Our docking studies also suggested that 3B5H10 recognizes fewer polyQ conformations than MW1. 3B5H10 appears to only bind compact conformations with two β-rich strands, but MW1 recognizes a wide range of exposed polyQ in soluble htt^{ex1}. Since 3B5H10 binding to htt^{ex1} predicts neurodegeneration significantly better than MW1 binding,[13] its prognostic value may reflect its higher specificity for a toxic conformer or closely related species.

Small-angle X-ray scattering confirms a compact two-stranded polyQ epitope recognized by 3B5H10

To experimentally test our docking predictions that 3B5H10 binds to a compact double-stranded conformation of polyQ, we used small-angle X-ray scattering (SAXS) to determine the shape of htt fragments in solution and in complex with 3B5H10 Fab. Htt fragments were expressed within six fusion proteins. The protein tags within the fusion proteins served two critical functions. First, as has been established, these tags help to prevent htt from aggregating, thus allowing analysis of substantially nonaggregated material too quickly.[5,36] Second, a series of protein tags, each of which has an

established crystal structure, allows us to accurately deduce the volume occupied by the polyQ stretch within the SAXS molecular envelope of htt or Fab/htt complexes. We reasoned that if six different htt fusion constructs all demonstrated a similar polyQ conformation, the chances that the protein tags were artificially altering the htt polyQ conformation were low.

The six fusion proteins used for our SAXS analysis included Thio-Htt^{ex1}-Q_{39}-His_6, which has been described previously. MBP-Htt^{ex1}-Q_{46}-Cer is a fusion protein of htt^{ex1} with a stretch of 46 glutamines, Cerulean fluorescent protein (Cer) at its C-terminus, and maltose binding protein (MBP) at its N-terminus. MBP-Htt$^{1–17}$-Q_{46}-Cer is similar but lacks the portion of htt^{ex1} after the polyQ stretch, which includes the proline-rich region. N-terminal tags from MBP-Htt^{ex1}-Q_{46}-Cer, MBP-Htt$^{1–17}$-Q_{46}-Cer, and Thio-Htt^{ex1}-Q_{39}-His_6 were removed proteolytically to generate the three remaining fusion constructs: Htt^{ex1}-Q_{46}-Cer, Htt$^{1–17}$-Q_{46}-Cer, and Htt^{ex1}-Q_{39}-His_6, respectively. By comparing SAXS

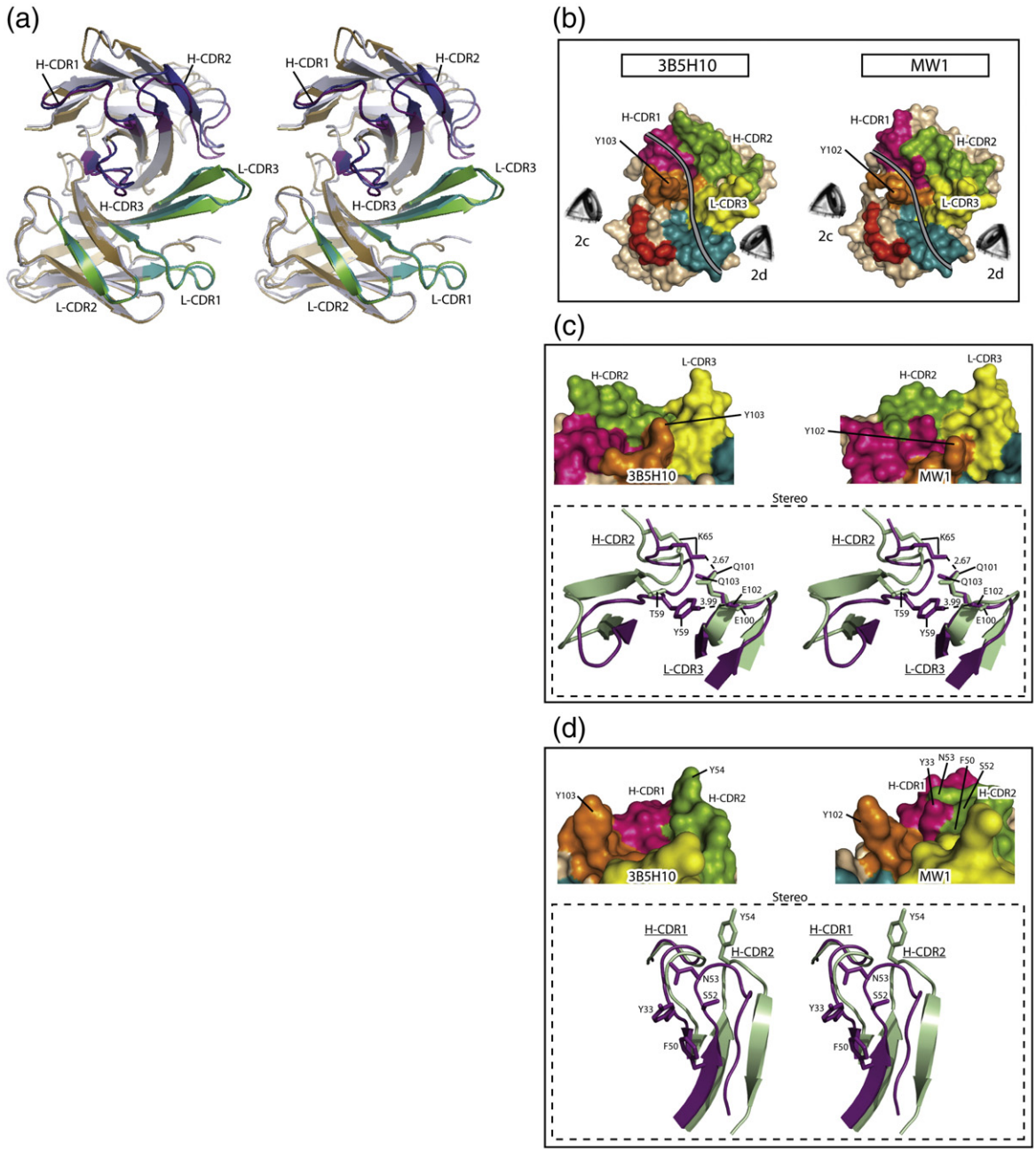

Fig. 2 (*legend on next page*)

data from fusion proteins with the same htt fragment but with different protein tags in the presence or in the absence of 3B5H10 Fab, we could assign regions of the molecular envelope to the tags, 3B5H10 Fab, and htt (Table S4 and Supplementary Methods).

Unlike 3B5H10 Fab/htt complexes containing MBP-Htt$^{1–17}$-Q_{46}-Cer or MBP-Htt^{ex1}-Q_{46}-Cer, the Fab/htt complex containing Thio-Htt^{ex1}-Q_{39}-His_6 is dimeric at the high concentrations used in SAXS.[13] The polyQ in the Thio-Htt^{ex1}-Q_{39}-His_6 complex SAXS envelope can be unambiguously assigned, but there are two possibilities for the path of the proline-rich region (Fig. S6). We favor one model (Fig. 4a) because it is consistent with the location of the proline-rich and Htt$^{1–17}$ regions in monomeric Htt^{ex1}-Q_{46}-Cer complexes and with the SAXS-derived structure of Thio-Htt^{ex1}-Q_{39}-His_6 in solution.

For all Fab/htt complexes tested, the htt fragment bends in the polyQ region, and the polyQ epitope in the complex is cylindrical, 24 Å in diameter, and 40–55 Å long. This compact volume is only consistent with a two-stranded hairpin structure and most consistent specifically with 16–24 glutamine residues in direct contact with the paratope of the Fab and a turn of 4–8 glutamine residues (Fig. 5a–c). The varying numbers of glutamines associated with the variable domain of Fab (24 for MBP-Htt$^{1–17}$-Q_{46}-Cer and 29 for MBP-Htt^{ex1}-Q_{39}-His_6 and MBP-Htt^{ex1}-Q_{46}-Cer) may reflect an influence of the proline-rich domain on the polyQ region.[37] However, SAXS analysis of Fab/htt complexes in which the proline-rich region or the N-terminal or C-terminal tags were removed also revealed a compact two-stranded hairpin-like structure for the polyQ region of htt (Table S4). Thus, compact hairpins appear to be an intrinsic property of the mutant polyQ stretch.

The compact two-stranded polyQ conformation recognized by 3B5H10 is abundant in solution

Having identified the structure of a polyQ conformation in htt that strongly predicts neurotoxicity, we sought to understand how abundant this conformation was in the absence of 3B5H10 using SAXS, circular dichroism (CD), and chemical cross-linking. SAXS and CD provide the population average of conformations sampled by a protein in solution, while cross-linking "freezes" the set of conformations that a protein samples at a given time. Thus, if the conformation that 3B5H10 recognizes is abundant in solution, SAXS and CD analyses of mutant htt unbound to an antibody should reveal a structure similar to the structure of mutant htt bound to the antibody. Additionally, cross-linking of mutant htt should preserve a strong subsequent binding by 3B5H10.

SAXS analysis of the htt fusion proteins unbound to 3B5H10 Fab revealed that the population average of polyQ conformers is best represented by a compact two-stranded hairpin structure that is highly similar to the conformation of polyQ bound to 3B5H10 (compare Fig. 5a–c and 5d–f). These findings are consistent with structural studies of smaller polyQ-containing peptides.[38] Furthermore, CD spectra of htt fusion proteins complexed to 3B5H10 Fab represent the simple sum of the CD spectra of the htt fusion proteins alone and the CD spectra of Fab alone (Fig. 5g; secondary structure analysis is shown in Fig. S7 and Supplementary

Fig. 2. Comparison of 3B5H10 and MW1 reveals key differences in the widths of the epitope binding grooves. (a) Stereo view of the superposition of 3B5H10 Fv (brown) and the Fv of unbound MW1 (PDB ID: 2GSG) (light gray). CDRs of 3B5H10 are shown in blue (heavy chain) and green (light chain). CDRs of MW1 are shown in purple (heavy chain) and cyan (light chain). 3B5H10 has significantly longer β-strands in H-CDR2 and L-CDR3 than MW1. (b–d) The structure of H-CDR2 determines the differences in the widths of the epitope binding groove between 3B5H10 and unbound MW1 (PDB ID: 2GSG). (b) Comparison of the antibody surfaces for 3B5H10 (left) and MW1 (right). H-CDR1, pink; H-CDR2, green; H-CDR3, orange; L-CDR1, cyan; L-CDR2, red; L-CDR3, yellow. The rest of the antibody is shown in tan. A gray line traces the epitope binding grooves in 3B5H10 and MW1. Y103 of 3B5H10 and Y102 of MW1 are noted to help facilitate structure orientation in (c) and (d). The eyes next to each structure indicate the line of sight for (c) and (d). (c) Zoomed-in view of the relationship between H-CDR2 and L-CDR3 for 3B5H10 (left) and MW1 (right), shown as in (b) and seen from the line of sight indicated by the eye labeled "2c" in (b). In MW1, H-CDR2 and L-CDR3 pack tightly against each other via two putative hydrogen bonds, forming a steep wall midway through one side of the epitope binding groove. In 3B5H10, H-CDR2 and L-CDR3 both form extended β-hairpins that do not significantly interact, leaving a more shallow and flexible wall midway through the analogous side of the epitope binding groove. This contributes to the wider diameter midway through 3B5H10's epitope binding groove than in MW1 (12.15 Å *versus* 5.5 Å). A stereo view of key hydrogen bonds between H-CDR2 and L-CDR3 in MW1 is presented at the bottom (broken lines). The corresponding regions of 3B5H10 (light green) are superimposed on MW1 (purple). (d) Zoomed-in view of the relationship between H-CDR2 and H-CDR1 for 3B5H10 (left) and MW1 (right), shown as in (b) and seen from the line of sight indicated by the eye labeled "2d" in (b). In MW1, H-CDR2 and H-CDR1 pack against each other to form a tall wall that severely restricts the width at one end of the epitope binding groove. In 3B5H10, the long β-hairpin of H-CDR2 pulls it away from H-CDR1, thereby widening the width of the epitope binding groove at the analogous end. A stereo view of the key residues in the H-CDR2/H-CDR1 interface that pack against each other in MW1 is presented at the bottom. The corresponding regions of 3B5H10 (light green) are superimposed on MW1 (purple). Y54 from H-CDR2 of 3B5H10 is noted for reference.

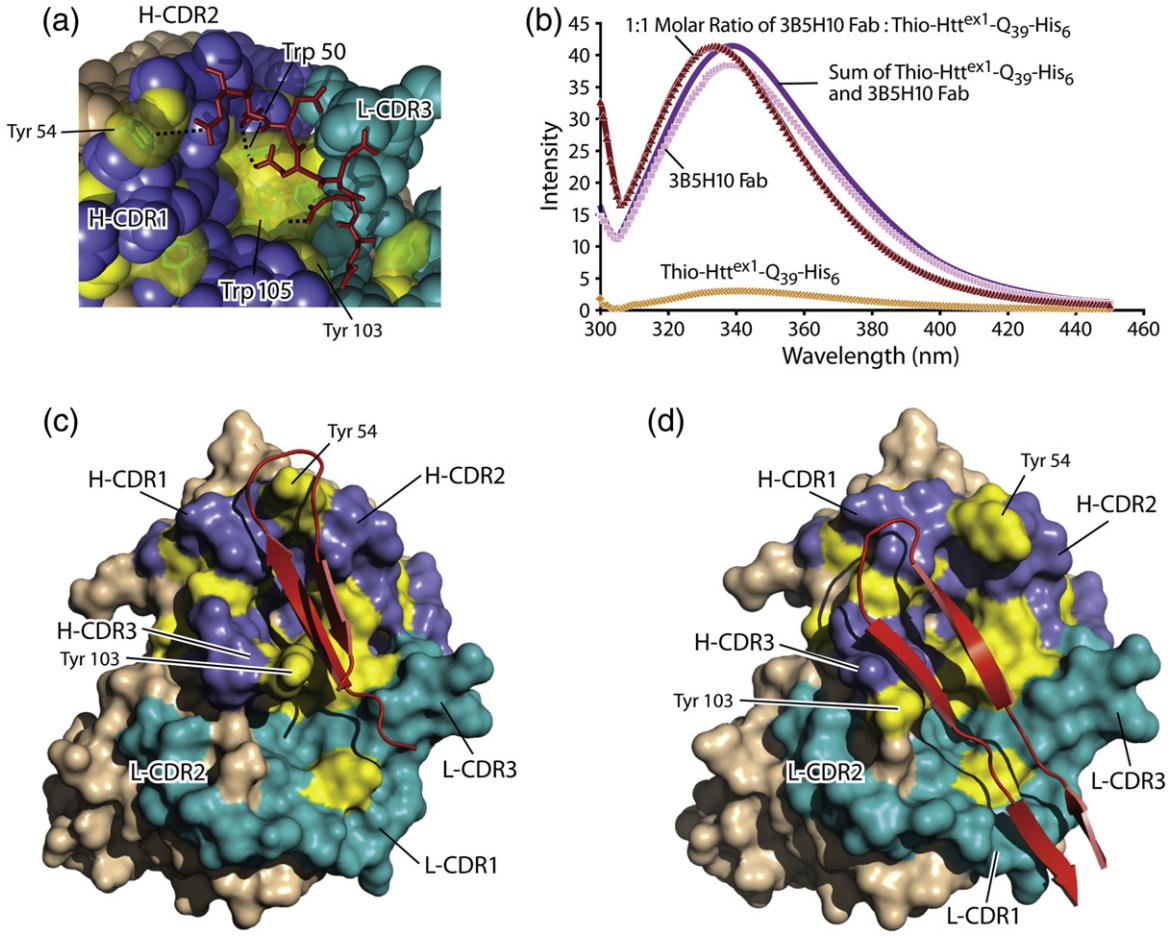

Fig. 3. Modeling reveals that polyQ binds into the 3B5H10 paratope as a compact two-stranded hairpin conformation. (a) Possible glutamine interactions in the central tryptophan pocket of 3B5H10's paratope. Solvent-accessible surfaces of the aromatic residues are shown in yellow, heavy-chain CDRs are shown in blue, and light-chain CDRs are shown in cyan. Central residues of the docked polyQ model (see model III in Fig. S3) are shown in red. Black dotted lines indicate potential hydrogen bonds between glutamines and tryptophans in the pocket and a potential π–π interaction between a glutamine side chain and a tyrosine from H-CDR2. (b) Fluorescence spectra of 3B5H10 Fab (pink), Thio-Htt^{ex1}-Q$_{39}$-His$_6$ (orange), and a 1:1 molar ratio of 3B5H10 Fab and Thio-Htt^{ex1}-Q$_{39}$-His$_6$ (red). The purple line is the sum of the 3B5H10 Fab and Thio-Htt^{ex1}-Q$_{39}$-His$_6$ spectra. The 5-nm shift indicates that binding reduces the polarity of the environment of some tryptophans in the complex. The only two solvent-accessible tryptophans are indicated (a). (c) β-Hairpin model of polyQ docked into the CDRs of the 3B5H10 crystal structure, shown as in (a) and with the portions of the polyQ model interacting with Fab (red ribbon). (d) β-Hairpin model of polyQ docked into the CDRs of 3B5H10 after domain rotation, shown as in (c). Domain rotation movement was analogous to that seen in MW1 upon peptide binding[2] and to other crystal forms of 3B5H10 (Fig. S2). This rotation widens and straightens the epitope binding groove so that it can accommodate a β-hairpin model with both strands submerged into the groove. Docking methods are summarized in Supplementary Methods. Goodness-of-fit parameters for the polyQ structures in (c) and (d) are presented in Fig. S4 as models III and II, respectively. MW1 and 3B5H10 docking studies are compared in the Supplementary Discussion.

Methods). Thus, the CD results demonstrate the lack of significant secondary structure change in htt upon 3B5H10 binding and confirm that 3B5H10 recognizes a secondary structure of mutant htt that represents the population average of polyQ conformers in unbound htt. In agreement with the SAXS and CD data, a strongly cross-linking mutant htt expressed in primary neurons with 4% paraformaldehyde and 0.2% glutaraldehyde, followed by 2% glutaraldehyde, results in robust subsequent antibody binding, as assessed by electron microscopy (Fig. S8). Collectively, these results are consistent with data demonstrating the ability of some proteins to sample several native conformations[39] and with 3B5H10 recognizing a conformation among those sampled by unaggregated htt.[40] Thus, we conclude that 3B5H10 recognizes a compact two-stranded hairpin

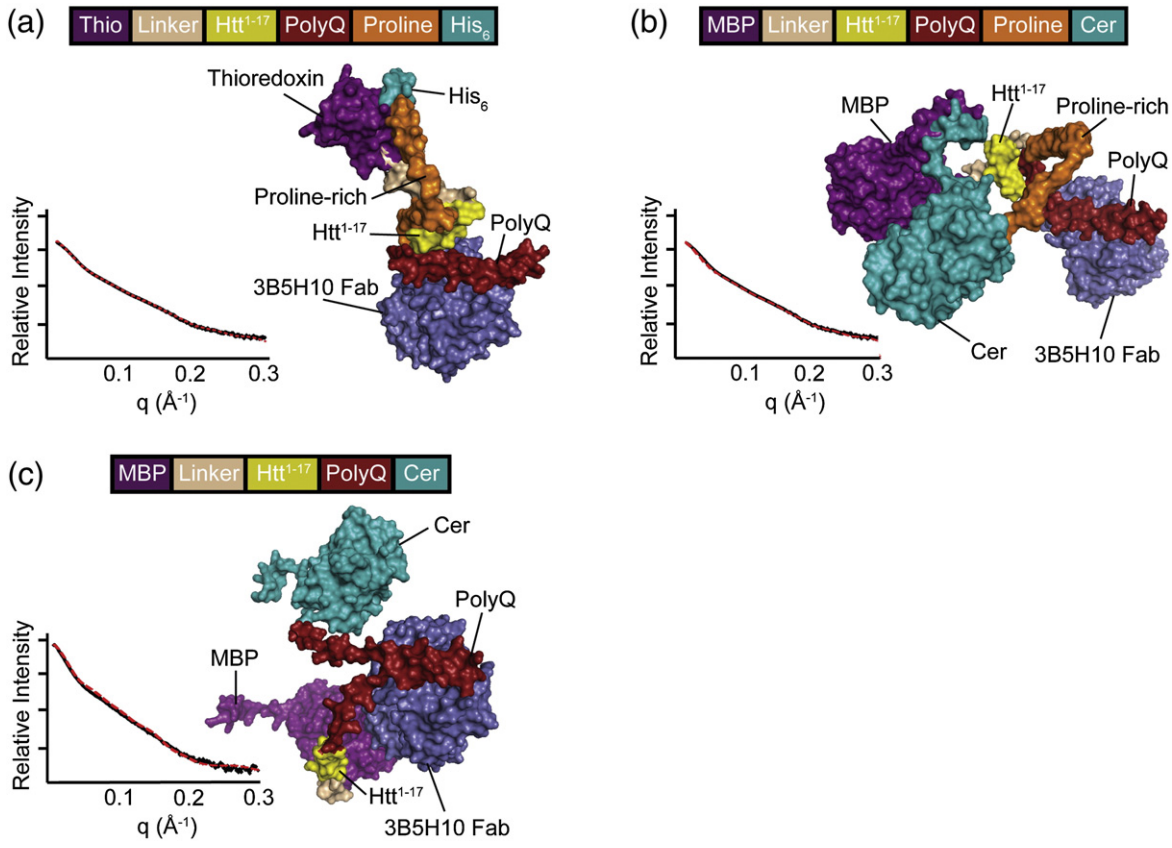

Fig. 4. SAXS confirms that 3B5H10 binds a compact two-stranded hairpin conformation of polyQ within mutant htt. (a) A monomeric htt^{ex1}/antibody complex from the Thio-Htt^{ex1}-Q_{39}-His_6/3B5H10 Fab dimer (Fig. S6). 3B5H10 Fab is shown in blue, thioredoxin is shown in purple, and the linker region between the thioredoxin and the N-terminus of htt is shown in tan. The 17 N-terminal residues of htt before the polyQ region ($htt^{1–17}$) are shown in yellow. PolyQ residues are shown in red, the proline-rich domain of htt is shown in orange, and the C-terminal His_6 tag is shown in cyan. A schema of the construct is presented on top. The graph (inset) shows the agreement between the observed SAXS curve (continuous, black) and the calculated SAXS curve (broken, red) of the preferred model (Fig. S6) ($\chi^2 = 1.8$). (b) The complex of MBP-Htt^{ex1}-Q_{46}-Cer and 3B5H10 Fab presented as in (a), except that the MBP is shown in purple and Cer is shown in cyan. The χ^2 between the SAXS data and the SAXS curve calculated from the model is 2.5. (c) The complex of MBP-$Htt^{1–17}$-Q_{46}-Cer and 3B5H10 Fab presented as in (b) ($\chi^2 = 2.0$).

conformation of polyQ that is abundant in solution and strongly predictive of neurodegeneration.

Discussion

In this study, we showed that polyQ stretches within monomeric mutant htt fragments form compact two-stranded hairpin structures in solution. This conformation, which represents the population average of conformations that mutant htt polyQ samples in solution, is recognized by a newly developed monoclonal antibody, 3B5H10. Since the epitope recognized by 3B5H10 predicts neurodegeneration better than all the other epitopes tested,[13] we propose that this polyQ structure has particular pathological significance.

That 3B5H10 binds a compact two-stranded hairpin structure of polyQ is supported by multiple lines of evidence. First, the epitope binding groove of 3B5H10 is at least twice as wide as the otherwise highly similar paratope on MW1, an antibody that accommodates only a single strand of polyQ. Molecular docking studies of polyQ structures into the paratope of MW1 *versus* 3B5H10 revealed that only compact two-stranded β-hairpin-rich structures of polyQ fit into 3B5H10. In contrast, MW1 accommodated a wide range of single-stranded polyQ structures, including the random-coil structure of the polyQ peptide that was cocrystallized with the antibody.[2] However, the MW1 paratope was unable to accommodate double-stranded polyQ structures, except when one strand was placed above and outside the paratope.

To further support that 3B5H10 binds polyQ in a β-strand conformation, others have introduced amino acid substitutions in the polyQ tract of htt whose nature and location were designed to disrupt

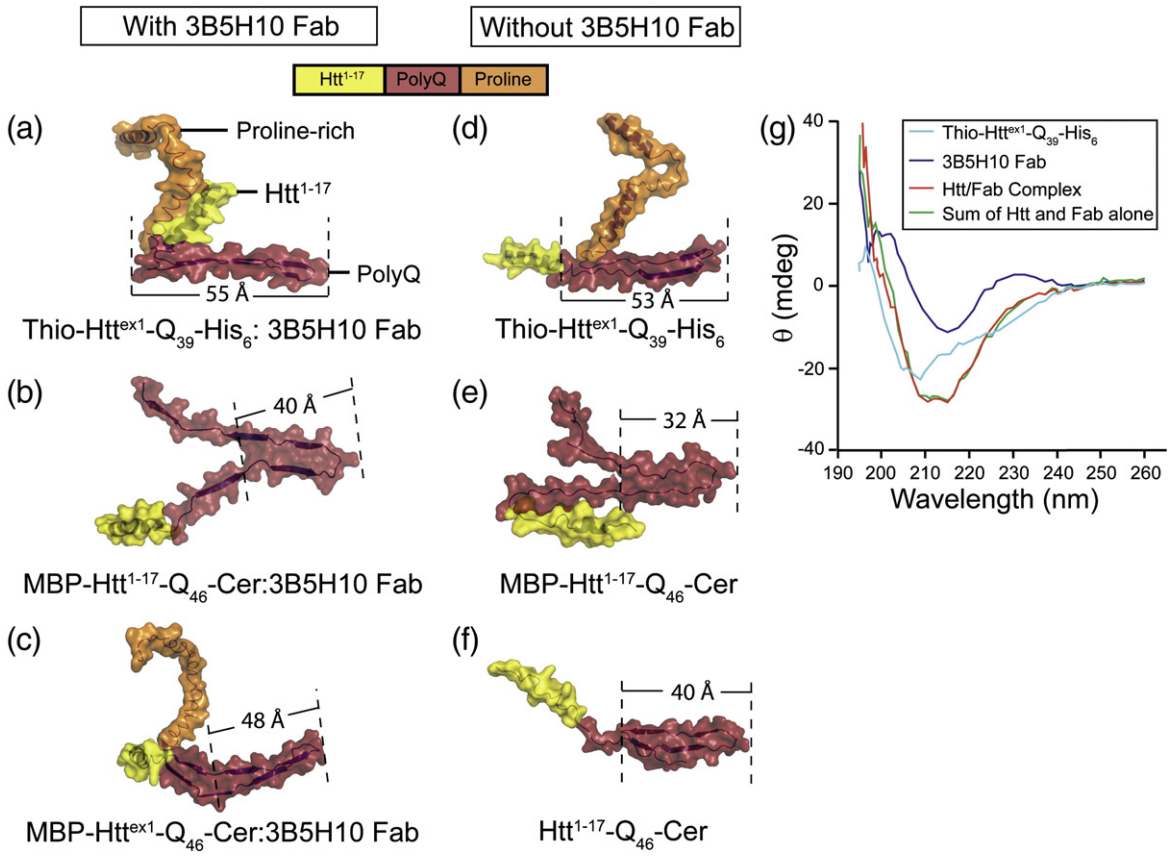

Fig. 5. 3B5H10 binds a polyQ conformation of mutant htt that is relatively abundant in solution. (a–f) Molecular envelopes of 3B5H10-bound and free htt fragments taken from the final SAXS models. A general schema for the constructs is presented on top. (a) Thio-Htt^{ex1}-Q$_{39}$-His$_6$ taken from its complex with 3B5H10 Fab. (b) MBP-Htt$^{1–17}$-Q$_{46}$-Cer taken from its complex with 3B5H10 Fab. (c) MBP-Htt^{ex1}-Q$_{46}$-Cer taken from its complex with 3B5H10 Fab. (d) Thio-Htt^{ex1}-Q$_{39}$-His$_6$ in solution (χ^2 = 1.5). (e) MBP-Htt$^{1–17}$-Q$_{46}$-Cer in solution (χ^2 = 1.9). (f) Htt$^{1–17}$-Q$_{46}$-Cer in solution (χ^2 = 1.7). The SAXS parameters for each model are summarized in Table S4. The mixture of β structure and random coil featured in the figure is only meant to illustrate a range of allowable structures consistent with the SAXS data and is not meant to represent a determined secondary structure (Supplementary Methods). However, a secondary structure containing at least some β character fits within SAXS envelopes better than secondary structures without any β-strand (Supplementary Methods). In all models, htt$^{1–17}$ is shown in yellow, the polyQ stretch is shown in red, and the proline-rich region is shown in orange. The SAXS data clearly indicate a highly similar compact polyQ hairpin for all htt fusion proteins (a–f), regardless of whether the htt fusion proteins are bound or unbound to 3B5H10 Fab (compare a–c *versus* d–f). (g) CD spectra for Thio-Htt^{ex1}-Q$_{39}$-His$_6$ alone, 3B5H10 Fab alone, or the complex of Thio-Htt^{ex1}-Q$_{39}$-His$_6$ bound to 3B5H10 Fab. The spectra from the complex match the spectrum of the sum of the htt spectra and the Fab spectra. These results, which show that there is no significant secondary structure change in htt or Fab upon complex formation, confirm that Fab binds to polyQ in a conformation representative of the average conformation of polyQ in solution. Similar results were obtained at different protein concentrations and using the MBP-Htt$^{1–17}$-Q$_{46}$-Cer fusion construct (Supplementary Methods). The secondary structure analysis for CD is shown in Fig. S7.

β structure. There was a correlation between the predicted disruption of β structure and reduced 3B5H10 binding.[41] Our SAXS data on a range of Fab/htt complexes confirmed predictions that 3B5H10 binds a compact two-stranded hairpin structure of polyQ. Furthermore, SAXS analysis, CD analysis, and chemical cross-linking experiments showed that the conformation recognized by 3B5H10 represents the population average of unbound htt in solution.[40] While our modeling suggests a predominantly β secondary structure to this compact conformation, molecular dynamics simulations and single-molecule force-clamp experiments indicate that a more disordered hairpin secondary structure in polyQ can also result in a compact ensemble of structures.[42,43]

Interestingly, MW1 and 3B5H10 both bind expanded polyQ stretches better than wt stretches, but their respective epitopes carry different prognostic values. Our docking studies of polyQ peptides into the MW1 paratope suggest that the paratope accommodates a wide range of single-stranded

polyQ structures. Thus, in agreement with previous studies, we conclude that MW1 is a polyQ binding protein rather than a conformation-specific protein. The antibody prefers longer polyQ stretches because they enable a more avid binding: the bivalent antibody dramatically increases binding when the short unstructured polyQ epitope it recognizes appears in tandem.[2,5]

In contrast, 3B5H10 is a conformation-specific antibody and therefore recognizes a much smaller range of htt species. Its preference for longer polyQ stretches is based on the recognition of a specific compact two-stranded hairpin conformation that emerges as the polyQ stretch expands. This specific conformation carries greater prognostic significance than the broader range of polyQ epitopes recognized by MW1. Interestingly, MW1 and 1C2 (another α-polyQ antibody that may bind polyQ according to the "linear lattice" model) were both raised against wt stretches of polyQ in different protein contexts. MW1 was raised against a 53-amino-acid fragment of wt atrophin-1-containing Q_{19}[44] (wt atrophin-1 contains $<Q_{49}$[45]). 1C2 was raised against the full-length wt TATA binding protein containing Q_{38}, the most common polyQ allelic variant in the human population[46–48] (wt TATA binding protein contains $<Q_{47}$[45]). In contrast, 3B5H10 was raised against a 171-amino-acid fragment of mutant htt (Q_{65}) prepared under native conditions (wt htt contains $<Q_{36}$[45]). Thus, the immunogens for MW1 and 1C2 would be expected to form the varied extended conformations characteristic of the wt stretches of polyQ. In contrast, the immunogen for 3B5H10 may form the more compact two-stranded hairpin conformation of mutant polyQ seen in our SAXS experiments on mutant htt fusion proteins unbound to antibody.

The compact conformation of mutant polyQ that we found for htt fusion proteins in solution unbound to antibody may seem surprising, as the polyQ stretch in purified Thio-Htt^{ex1}-Q_{39}-His_6 reportedly has an extended linear conformation.[5] Furthermore, the possibility of extensive stable regions of α or β secondary structure in polyQ peptides have been ruled out through CD and nuclear magnetic resonance analyses, suggesting that the polyQ stretch adopts a random-coil conformation.[5] Our SAXS analysis also indicates that Htt^{ex1}-Q_{39} lacks a stable secondary structure. For example, the Kratky plot of Thio-Htt^{ex1}-Q_{39}-His_6 in solution has the typical shape of a protein with an extensive unfolded region (Fig. S9). Similarly, the maximum dimension of Thio-Htt^{ex1}-Q_{39}-His_6 from SAXS (140 ± 10 Å) would be within experimental error of the predicted length of the protein (130 Å) if it were a random coil[49] (Table S4). Finally, the calculated molecular volume of Thio-Htt^{ex1}-Q_{39}-His_6 is 1.5 ± 0.2 times the volume expected for a globular protein (Table S4). This volume is within the range typical of other proteins, in which 40–50% of the residues are predicted to be unfolded.[50] Thus, in aggregate, our data suggest that the polyQ stretch in mutant htt samples many conformations when unbound to an antibody, failing to form any consistent stable secondary structure. However, the population average of these transiently sampled conformations is best represented by a compact two-stranded hairpin conformation.

In summary, we present experimental evidence of a compact two-stranded hairpin conformation of polyQ in htt fragments containing polyQ stretches long enough to cause neurodegeneration. This structure, which is abundant in htt fragments unbound by antibody, is recognized by a newly developed monoclonal antibody, 3B5H10. Since 3B5H10 binding predicts neurodegeneration better than MW1 binding,[13] this conformation may be neurotoxic. How this structure might lead to neurodegeneration is unclear. The pair of polyQ strands could be part of a structure that interacts with certain intracellular proteins or lipids, sequestering or regulating their function in deleterious ways.[1] Alternatively, the polyQ conformation could alter the normal functions of the proteins that contain them (e.g., htt), resulting in toxicity. If the length of the polyQ stretch partly governs the distribution of conformers,[39] it could explain how versions of these proteins with wt polyQ stretches can sometimes cause neurodegeneration when overexpressed.[51,52] Finally, while our data demonstrate that the 3B5H10 epitope appears predominantly on monomeric htt,[13] if the conformation is exposed and available for interaction in aggregated proteins under certain unique circumstances,[53] the conformation may mediate pathogenesis in such circumstances as well. If inclusion body formation then reduces the specific activity of these toxic conformers by sequestration or refolding, it could explain how inclusion body formation improves survival.[54,55]

Materials and Methods

Crystal structure of 3B5H10 Fab

Purification, sequencing, and crystallization of 3B5H10 Fab are described in the Supplementary Methods.

Solution of crystal forms

Data collection and solutions for the orthorhombic (not deposited), monoclinic (PDB ID: 3S96), and alternate (PDB ID: 4DCQ) crystal forms of 3B5H10 Fab are described in the Supplementary Methods (Tables S1–S3). The final R_{work} and R_{free} values for the monoclinic model (refined from 11 Å to 1.90 Å) were 0.19 and 0.26, respectively (PDB ID: 3S96).

SAXS data collection

Purified fusion protein constructs used for SAXS are described in Supplementary Methods. SAXS data were collected using protein concentrations in the range of 1–5 mg/ml and an X-ray wavelength of 1.11 Å at beamline 12.3.1 (Advanced Light Source) or beamline 4-2 (Stanford Synchrotron Radiation Laboratory). Samples of the running buffer from the size-exclusion columns used to purify proteins and protein complexes for SAXS analysis were used for buffer subtraction. Data were integrated with software customized for each beamline and processed with the program PRIMUS.[56] The program GNOM[57] was used to calculate the maximum dimension and the radius of gyration and to estimate the intensity of scattering at zero angle. The dimensional data for each sample are summarized in Table S4. No significant differences were observed in the dimensional data across the concentration ranges tested for each sample. SAXS data were analyzed as described in Supplementary Methods.

Circular dichroism

Proteins were prepared in phosphate-buffered saline and allowed to incubate together for at least 30 min at room temperature before the CD spectrum was measured. The complex of Thio-Htt^{ex1}-Q_{39}-His_6 and 3B5H10 Fab was formed in a 1:1 stoichiometry. The protein concentrations for the experiment were 55 μg/ml Thio-Htt^{ex1}-Q_{39}-His_6 and 95 μg/ml 3B5H10 Fab. The experiments were also repeated using 110 μg/ml Thio-Htt^{ex1}-Q_{39}-His_6 and 190 μg/ml Fab, with the same results. A similar analysis was performed on MBP-Htt^{ex1}-Q_{46}-Cer and Fab at two different protein concentrations (data not shown). Conclusions from the MBP-Htt^{ex1}-Q_{46}-Cer experiments mirror conclusions from the Thio-Htt^{ex1}-Q_{39}-His_6 experiments. CD was performed under standard conditions using a Jasco J-810 instrument. CD data analysis is presented in Fig. S7 and the Supplementary Methods.

Cross-linking and electron microscopy

Striatal neurons transfected with Htt^{ex1}-Q_{46} C-terminally tagged with enhanced green fluorescent protein were fixed for 15 min in a solution of 4% paraformaldehyde and 0.2% glutaraldehyde. Plates were then fixed in 2% glutaraldehyde in 0.1 M cacodylate buffer (pH 7.4) at room temperature for 2 min, placed on ice for 30 min, washed with 0.1 M cacodylate buffer, and postfixed with 1% osmium tetraoxide for 30 min. Cells were then prepared for electron microscopy in standard fashion, sectioned into 60-nm slices, and imaged on a Zeiss EM10 electron microscope (Supplementary Methods).

Accession numbers

The coordinates of the monoclinic form of 3B5H10 presented in the text have been deposited in the PDB under PDB ID 3S96 and Research Collaboratory for Structural Bioinformatics ID RCSB065918. The alternate crystal form of 3B5H10 (Fig. S2e) has been assigned under PDB ID 4DCQ and Research Collaboratory for Structural Bioinformatics ID RCSB070164.

Supplementary materials related to this article can be found online at doi:10.1016/j.jmb.2012.01.034

Acknowledgements

We thank P. Bjorkman for the Thio-Htt^{ex1}-Q_{39}-His_6 plasmid, D. Minor (University of California San Francisco) for the pET28-HMT and pTEV vectors, and Raymond Boynton (N-Terminal Protein Sequencing Facility, Biogen, Inc.) for assistance with N-terminal deblocking and sequencing of the 3B5H10 heavy-chain and light-chain polypeptides. We thank the members of the Finkbeiner and Weisgraber laboratories for discussions; Greg Hura, Ken Frankel, and Thomas Weiss for assistance with SAXS data collection; Stephen Ordway and Gary Howard for editorial assistance; Kelley Nelson for administrative assistance; and Margaret Sutherland and Diane Murphy for their interest and support. Primary support for this work was provided by the CHDI Foundation, Inc. (S.F.), the National Institute on Aging (S.F.), and the National Institute of Neurological Disorders and Stroke (S.F.). Additional support was provided by the Taube Family Foundation Program in Huntington's Disease Research, a Therapeutics Initiative Award from the Huntington's Disease Society of America, the National Center for Research Resources, and the J. David Gladstone Institutes (S.F.). M.A. and J.M. were supported by the Hillblom Foundation. S.M. and J.M. were supported by the National Institutes of Health National Institute of General Medical Sciences University of California San Francisco Medical Scientist Training Program. J.M. was supported by a fellowship from the University of California Graduate Division Achievement Rewards for College Scientists. Crystallographic and SAXS data were collected through the general user program at the Advanced Light Source and the Stanford Synchrotron Radiation Laboratory. K.H.W. was supported by National Institutes of Health grants HL-64963 and AG-020235. S.F. was supported by National Institutes of Health grants NS-039074, NS-045191, and AG-022074.

References

1. Schaffer, G., Breuer, P., Boteva, R., Behrends, C., Tzetkov, K., Stripple, N. *et al.* (2004). Cellular toxicity of polyglutamine expansion proteins: mechanism of transcription factor deactivation. *Mol. Cell*, **15**, 95–105.
2. Li, P., Huey-Tubman, K. E., Gao, T., Li, X., West, A. P., Jr., Bennett, M. J. & Bjorkman, P. J. (2007). The structure of a polyQ–anti-polyQ complex reveals binding according to a linear lattice model. *Nat. Struct. Mol. Biol.* **14**, 381–387.

3. Nagai, Y., Tucker, T., Ren, H., Kenan, D. J., Henderson, B. S., Keene, J. D. *et al.* (2000). Inhibition of polyglutamine protein aggregation and cell death by novel peptides identified by phage display screening. *J. Biol. Chem.* **275**, 10437–10442.
4. May, B. C. H., Fafarman, A. T., Hong, S. B., Rogers, M., Deady, L. W., Prusiner, S. B. & Cohen, F. E. (2003). Potent inhibition of scrapie prion replication in cultured cells by bis-acridines. *Proc. Natl Acad. Sci. USA*, **100**, 3416–3421.
5. Bennett, M. J., Huey-Tubman, K. E., Herr, A. B., West, A. P., Jr., Ross, S. A. & Bjorkman, P. J. (2002). A linear lattice model for polyglutamine in CAG-expansion diseases. *Proc. Natl Acad. Sci. USA*, **99**, 11634–11639.
6. Perutz, M. F., Finch, J. T., Berriman, J. & Lesk, A. (2002). Amyloid fibers are water-filled nanotubes. *Proc. Natl Acad. Sci. USA*, **99**, 5591–5595.
7. Kim, M. W., Chelliah, Y., Kim, S. W., Otwinowski, Z. & Bezprozvanny, I. (2009). Secondary structure of Huntingtin amino-terminal region. *Structure*, **17**, 1205–1212.
8. Jayaraman, M., Kodali, R., Sahoo, B., Thakur, A. K., Mayasundari, A., Mishra, R. *et al.* (2011). Slow amyloid nucleation via α-helix-rich oligomeric intermediates in short polyglutamine-containing huntingtin fragments. *J. Mol. Biol.* E-publication ahead of print.
9. Saunders, H. M. & Bottomley, S. P. (2009). Multi-domain misfolding: understanding the aggregation pathway of polyglutamine proteins. *Protein Eng. Des. Sel.* **22**, 447–451.
10. Klein, F. A. C., Pastore, A., Masino, L., Zeder-Lutz, G., Nierengarten, H., Oulad-Abdelghani, M. *et al.* (2007). Pathogenic and non-pathogenic polyglutamine tracts have similar structural properties: towards a length-dependent toxicity gradient. *J. Mol. Biol.* **371**, 235–244.
11. Legleiter, J., Lotz, G. P., Miller, J., Ko, J., Ng, C., Williams, G. L. *et al.* (2009). Monoclonal antibodies recognize distinct conformational epitopes formed by polyglutamine in a mutant huntingtin fragment. *J. Biol. Chem.* **284**, 21647–21658.
12. Nagai, Y., Inui, T., Popiel, H. A., Fujikake, N., Hasegawa, K., Urade, Y. *et al.* (2007). A toxic monomeric conformer of the polyglutamine protein. *Nat. Struct. Mol. Biol.* **14**, 332–340.
13. Miller, J., Arrasate, M., Brooks, E., Libeu, C. P., Legleiter, J., Hatters, D. *et al.* (2011). Identifying polyglutamine proteins species *in situ* that best predict neurodegeneration. *Nat. Chem. Biol.* **7**, 925–934.
14. Watkins, W. S., Bamshad, M. & Jorde, L. B. (1995). Population genetics of trinucleotide repeat polymorphisms. *Hum. Mol. Genet.* **4**, 1485–1491.
15. Barron, L. H., Warner, J. P., Porteous, M., Holloway, S., Simpson, S., Davidson, R. & Brock, D. J. H. (1993). A study of the Huntington's disease associated trinucleotide repeat in the Scottish population. *J. Med. Genet.* **30**, 1003–1007.
16. Pramanik, S., Basu, P., Gangopadhaya, P. K., Sinha, K. K., Jha, D. K., Sinha, S. *et al.* (2000). Analysis of CAG and CCG repeats in *Huntingtin* gene among HD patients and normal populations of India. *Eur. J. Hum. Genet.* **8**, 678–682.
17. Costa, M. C., Magalhaes, P., Guimaraes, L., Maciel, P., Sequeiros, J. & Sousa, A. (2006). The CAG repeat at the Huntington disease gene in the Portuguese population: insights into its dynamics and to the origin of the mutation. *J. Hum. Genet.* **51**, 189–195.
18. Duncan, M. J., Mann, E. L., Cohen, M. S., Ofek, I., Sharon, N. & Abraham, S. N. (2005). The distinct binding specificities exhibited by enterobacterial type 1 fimbriae are determined by their fimbrial shafts. *J. Biol. Chem.* **280**, 37707–37716.
19. Hubbard, M. J. & Klee, C. B. (1987). Calmodulin binding by calcineurin. Ligand-induced renaturation of protein immobilized on nitrocellulose. *J. Biol. Chem.* **262**, 15062–15070.
20. Birk, H. W. & Koepsell, H. (1987). Reaction of monoclonal antibodies with plasma membrane proteins after binding on nitrocellulose: renaturation of antigenic sites and reduction of nonspecific antibody binding. *Anal. Biochem.* **164**, 12–22.
21. Celenza, J. L. & Carlson, M. (1991). Renaturation of protein kinase activity of protein blots. *Methods Enzymol.* **200**, 423–430.
22. Fischer, R., Wei, Y. & Berchtold, M. (1996). Detection of calmodulin-binding proteins using a ^{32}P-labeled GST–calmodulin fusion protein and a novel renaturation protocol. *BioTechniques*, **21**, 292–296.
23. Klinz, F. J. (1994). GTP-blot analysis of small GTP-binding proteins. The C-terminus is involved in renaturation of blotted proteins. *Eur. J. Biochem.* **225**, 99–105.
24. Shackelford, D. A. & Zivin, J. A. (1993). Renaturation of calcium/calmodulin-dependent protein kinase activity after electrophoretic transfer from sodium dodecyl sulfate–polyacrylamide gels to membranes. *Anal. Biochem.* **211**, 131–138.
25. Zeng, F. Y., Oka, J. A. & Weigel, P. H. (1996). Renaturation and ligand blotting of the major subunit of the rat asialoglycoprotein receptor after denaturing polyacrylamide gel electrophoresis. *Glycobiology*, **6**, 247–255.
26. Brooks, E., Arrasate, M., Cheung, K. & Finkbeiner, S. M. (2004). Using antibodies to analyze polyglutamine stretches. *Methods Mol. Biol.* **277**, 103–128.
27. Peters-Libeu, C., Newhouse, Y., Krishnan, P., Cheung, K., Brooks, E., Weisgraber, K. & Finkbeiner, S. (2005). Crystallization and diffraction properties of the Fab fragment of 3B5H10, an antibody specific for disease-causing polyglutamine stretches. *Acta Crystallogr., Sect. F: Struct. Biol. Cryst. Commun.* **61**, 1065–1068.
28. Eisen, H. N. & Reilly, E. B. (1985). Lambda chains and genes in inbred mice. *Annu. Rev. Immunol.* **3**, 337–365.
29. Zhang, X., Smith, D. L., Meriin, A. B., Engemann, S., Russel, D. E., Roark, M. *et al.* (2005). A potent small molecule inhibits polyglutamine aggregation in Huntington's disease neurons and suppresses neurodegeneration *in vivo*. *Proc. Natl Acad. Sci. USA*, **102**, 892–897.
30. Nagai, Y., Fujikake, N., Ohno, K., Higashiyama, H., Popiel, H. A., Rahadian, J. *et al.* (2003). Prevention of polyglutamine oligomerization and neurodegeneration by the peptide inhibitor QBP1 in *Drosophila*. *Hum. Mol. Genet.* **12**, 1253–1259.
31. Stanfield, R. L., Takimoto-Kamimura, M., Rini, J. M., Profy, A. T. & Wilson, I. A. (1993). Major antigen-induced domain rearrangements in an antibody. *Structure*, **1**, 83–93.

32. Sundberg, E. J. & Mariuzza, R. A. (2002). Molecular recognition in antibody–antigen complexes. *Adv. Protein Chem.* **61**, 119–160.
33. Ross, C. A., Poirier, M. A., Wanker, E. E. & Amzel, M. (2003). Polyglutamine fibrillogenesis: the pathway unfolds. *Proc. Natl Acad. Sci. USA*, **100**, 1–3.
34. Comeau, S. R., Gatchell, D. W., Vajda, S. & Camacho, C. J. (2004). ClusPro: an automated docking and discrimination method for the prediction of protein complexes. *Bioinformatics*, **20**, 45–50.
35. Chen, R., Li, L. & Weng, Z. (2003). ZDOCK: an initial-stage protein-docking algorithm. *Proteins*, **52**, 80–87.
36. Poirier, M. A., Li, H., Macosko, J., Cai, S., Amzel, M. & Ross, C. A. (2002). Huntingtin spheroids and protofibrils as precursors in polyglutamine fibrillization. *J. Biol. Chem.* **277**, 41032–41037.
37. Bhattacharyya, A., Thakur, A. K., Chellgren, V. M., Thiagarajan, G., Williams, A. D., Chellgren, B. W. *et al.* (2006). Oligoproline effects on polyglutamine conformation and aggregation. *J. Mol. Biol.* **355**, 524–535.
38. Perutz, M. F., Johnson, T., Suzuki, M. & Finch, J. T. (1994). Glutamine repeats as polar zippers: their possible role in inherited neurodegenerative diseases. *Proc. Natl Acad. Sci. USA*, **91**, 5355–5358.
39. Tuinstra, R. L., Peterson, F. C., Kutlesa, S., Elgin, E. S., Kron, M. A. & Volkman, B. F. (2008). Interconversion between two unrelated protein folds in the lymphotactin native state. *Proc. Natl Acad. Sci. USA*, **105**, 5057–5062.
40. Lange, O. F., Lakomek, N. A., Farès, C., Schröder, G. F., Walter, K. F. A., Becker, S. *et al.* (2008). Recognition dynamics up to microseconds revealed from an RDC-derived ubiquitin ensemble in solution. *Science*, **320**, 1471–1475.
41. Zhang, Q. C., Yeh, T. L., Leyva, A., Frank, L. G., Miller, J., Kim, Y. E. *et al.* (2011). A compact β model of huntingtin toxicity. *J. Biol. Chem.* **286**, 8188–8196.
42. Wang, X., Vitalis, A., Wyczalkowski, M. A. & Pappu, R. V. (2006). Characterizing the conformational ensemble of monomeric polyglutamine. *Proteins*, **63**, 297–311.
43. Dougan, L., Li, J., Badilla, C. L., Berne, B. J. & Fernandez, J. M. (2009). Single homopolypeptide chains collapse into mechanically rigid conformations. *Proc. Natl Acad. Sci. USA*, **106**, 12605–12610.
44. Ko, J., Ou, S. & Patterson, P. H. (2001). New anti-huntingtin monoclonal antibodies: implications for huntingtin conformation and its binding proteins. *Brain Res. Bull.* **56**, 319–329.
45. Williams, A. J. & Paulson, H. L. (2008). Polyglutamine neurodegeneration: protein misfolding revisited. *Trends Neurosci.* **31**, 521–528.
46. Trottier, Y., Lutz, Y., Stevanin, G., Imbert, G., Devys, D., Cancel, G. *et al.* (1995). Polyglutamine expansion as a pathological epitope in Huntington's disease and four dominant cerebellar ataxias. *Nature*, **378**, 403–406.
47. Lescure, A., Lutz, Y., Eberhard, D., Jacq, X., Krol, A., Grummt, I. *et al.* (1994). The N-terminal domain of the human TATA-binding protein plays a role in transcription from TATA-containing polymerase II and III promoters. *EMBO J.* **13**, 1166–1175.
48. Brou, C., Chaudhary, S., Davidson, I., Lutz, Y., Wu, J., Egly, J. M. *et al.* (1993). Distinct TFIID complexes mediate the effect of different transcriptional activators. *EMBO J.* **12**, 489–499.
49. Tanford, C. (1970). Protein denaturation: C. Theoretical models for the mechanism of denaturation. *Adv. Protein Chem.* **24**, 1–95.
50. Uversky, V. N. (2002). Natively unfolded proteins: a point where biology waits for physics. *Protein Sci.* **11**, 739–756.
51. Fernandez-Funez, P., Nino-Rosales, M. L., de Gouyon, B., She, W. C., Luchak, J. M., Martinez, P. *et al.* (2000). Identification of genes that modify ataxin-1-induced neurodegeneration. *Nature*, **408**, 101–106.
52. Yoo, S. Y., Pennesi, M. E., Weeber, E. J., Xu, B., Atkinson, R., Chen, S. *et al.* (2003). SCA7 knockin mice model human SCA7 and reveal gradual accumulation of mutant ataxin-7 in neurons and abnormalities in short-term plasticity. *Neuron*, **37**, 383–401.
53. Nekooki-Machida, Y., Kurosawa, M., Nukina, N., Ito, K., Oda, T. & Tanaka, M. (2009). Distinct conformations of *in vitro* and *in vivo* amyloids of huntingtin–exon1 show different cytotoxicity. *Proc. Natl Acad. Sci. USA*, **106**, 9679–9684.
54. Arrasate, M., Mitra, S., Schweitzer, E. S., Segal, M. R. & Finkbeiner, S. (2004). Inclusion body formation reduces levels of mutant huntingtin and the risk of neuronal death. *Nature*, **431**, 805–810.
55. Saudou, F., Finkbeiner, S., Devys, D. & Greenberg, M. E. (1998). Huntingtin acts in the nucleus to induce apoptosis, but death does not correlate with the formation of intranuclear inclusions. *Cell*, **95**, 55–66.
56. Konarev, P. V., Volkov, V. V., Sokolova, A. V., Koch, M. H. & Svergun, D. I. (2003). PRIMUS: a Windows PC-based system for small-angle scattering data analysis. *J. Appl. Crystallogr.* **36**, 1277–1282.
57. Svergun, D. I. (1992). Determination of the regularization parameter in indirect-transform methods using perceptual criteria. *J. Appl. Crystallogr.* **25**, 495–503.

Glossary

Paratope: The antigen binding site of an antibody that is usually composed of the complementarity-determining regions of the heavy and light chains from the Fv region.
Polyglutamine disease: One of nine neurodegenerative disorders caused by the expansion of a polyglutamine stretch beyond a well-defined threshold length in otherwise nonhomologous proteins.
Huntingtin: A 350-kDa protein with a polyglutamine stretch near the N-terminus. The protein is expressed in all tissues, but expansion of the polyglutamine stretch beyond 36Q (mutant htt) specifically triggers neurodegeneration. Expansion also triggers the accumulation of the proteolytically cleaved N-terminal fragments of the protein containing the polyglutamine stretch. Htt has myriad postulated functions (from scaffolding to cellular transport to transcriptional regulation to energy homeostasis), and its knockout is embryo lethal.
3B5H10: A novel monoclonal antibody developed by our laboratory against an N-terminal fragment of mutant htt that recognizes the protein in a polyglutamine-dependent manner.
MW1: A monoclonal antibody developed by the Patterson laboratory at CalTech against a small fragment of wild-type atrophin-1, a polyglutamine-containing protein. While raised against wild-type atrophin, the antibody recognizes mutant htt in a polyglutamine-dependent manner.